Comparison of three DWM-based wake models at above-rated wind speeds

Ø W Hanssen-Bauer[1], P Doubrawa[2], H Aa Madsen[3], H Asmuth[4], J Jonkman[2], G C Larsen[3], S Ivanell[4] and R Stenbro[1]

[1] Institute for Energy Technology, Instituttveien 18, 2007 Kjeller, Norway
[2] National Renewable Energy Laboratory, Golden, CO 80401, USA
[3] Department of Wind Energy, Risø Campus, Technical University of Denmark, DK-4000 Roskilde, Denmark
[4] Wind Energy Section, Department of Earth Sciences, Uppsala University Campus Gotland, 621 67 Visby, Sweden

E-mail: oyvind.hanssen-bauer@ife.no

Abstract. In this study we investigate three mid-fidelity wind turbine wake models based on the dynamic wake meandering (DWM) model principle, and compare their performance with a reference dataset, produced with large-eddy simulations using the actuator line model. The models are compared with respect to flow field, power, and loads on a row of four 5MW reference turbines experiencing above-rated wind conditions. In general, the DWM models show fairly good agreement with large-eddy simulation for the time-averaged flow fields, blade forces and power, with increasing differences along the turbine row. Also when comparing fatigue loads of blade root moments, the differences between the models increase further into the row, with deviations up to 25 % of the reference case. However, while the development in blade root moment fatigue along the turbine row is predominantly driven by the energy content at the frequency corresponding to the turbine's rotational period ($1P$) for the DWM models, the large-eddy simulation results suggest that the key drivers for the blade root and tower loads are the increase in meandering and energy at higher frequencies ($> 1P$) deeper into the turbine row. For the tower loads, the DWM models highly underestimate the fatigue for the waked turbines. From these results, we suggest priorities for future model developments so that robust model implementations can be used in wind farm design and operation.

1. Introduction

Accurate calculation of turbine power and loads under all the various conditions the turbines are facing during their lifetime is important in both the design process and during the operation of wind farms. Simpler engineering models like the Jensen and Frandsen model [1, 2], and even Reynolds-averaged Navier-Stokes computational fluid dynamics (CFD), do not capture temporal variations in wake flows and are consequently insufficient for load calculations. High-fidelity CFD models like large-eddy simulations (LES) are too computationally expensive to cover all relevant load cases for a whole wind park, where the position of the individual wind turbines affects what wind conditions they experience over the life span. Particularly, at above-rated wind speeds it is important to accurately estimate the wake flow, as the load levels have shown to increase significantly for multi-wake situations [3]. The Dynamic Wake Meandering (DWM) model [4, 5], which has been included in the new edition of the International Electrotechnical Commisions

code as a recommended practice [6], captures most of the essential physics of wind farm flow fields and is therefore an interesting compromise between accuracy and computational demand. When this model is coupled to an aeroelastic solver, turbine loads can also be estimated. Since the introduction of the DWM model, several improvements to the original formulation have been suggested and other wake models based on the main DWM ideas have been developed [7, 8, 9, 10]. In this study, two such models are compared against the original DWM model and against high-fidelity LES.

2. Methodology

2.1. The DWM models

The original DWM model is based on the assumption that the quasi-steady wake deficit, obtained from a thin shear-layer approximation of the Navier-Stokes equations, meanders in a stochastic manner due to the large-scale turbulent structures in the wind. A homogeneous Mann turbulence field [11, 12] with a box grid size of one turbine diameter (D) and turbulence intensity (TI) as ambient turbulence is used for derivation of the meandering. The initial velocity profile behind the turbine comes from the blade element momentum (BEM) model but is adjusted by including a simple closed-form modification taking care of the pressure recovery in the wake near field. Self-generated turbulence in the wake of the turbines comes in addition to conventional atmospheric boundary layer turbulence. In practice the wake self-generated turbulence is modeled based on an isotropic Mann box with smaller length scale [1] than the conventional inflow turbulence.

For multiple wake situations, where a turbine's incoming flow field is affected by more than one wake of upstream turbines, it was originally suggested to use the maximum deficit operator described in [13] to account for waked inflow conditions for all wind speed regimes to estimate the incoming velocity for power and load calculations of a turbine. The maximum deficit operator looks at the wake deficit from each upstream turbine when operating in isolation (i.e., experiencing freestream velocity), and assumes that the total incoming wake deficit can be approximated to be the maximum single wake deficit, evaluated at each radial position of the turbine of interest. In a later study [3] it was decided to distinguish between below- and above-rated wind speeds, and for the latter case use a linear summation of the wake deficits. This linear approximation is obtained from assuming the upstream turbines are operating in isolation and was first suggested by Lissaman [14] for situations with weak wake interaction. This is consistent with above-rated operation, where the wake effects gradually decrease.

In this study, we compare three different DWM-based wake models. Both $\mathrm{DWM_{DTU,\ Mann}}$ and $\mathrm{DWM_{DTU}}$ use the original DWM model developed at the Technical University of Denmark (DTU), but differ in the way that the meandering is treated. The second model uses the National Renewable Energy Laboratory (NREL) DWM implementation in FAST.Farm, named $\mathrm{DWM_{NREL}}$ in this study. Finally, the third model, named $\mathrm{DWM_{IFE}}$, uses the DWM implementation WIFET Farm from Institute for Energy Technology (IFE). Here we explain the differences in each of these simulation approaches.

The $\mathrm{DWM_{DTU,\ Mann}}$ model uses the original Mann box approach for derivation of the meandering, which the model parameters previously have been calibrated for. Therefore $\mathrm{DWM_{DTU,\ Mann}}$ was run with default model parameter settings in this study. The rest of the DWM models compared in this study use a different incoming wind field, an LES-generated precursor that will be further described in section 2.2. $\mathrm{DWM_{DTU}}$ was run with an increased coupling factor of eddy viscosity to ambient turbulence, as it was found that the meandering from the LES precursor flow field was lower when using the Mann box approach.

FAST.Farm, which is developed at the NREL [8, 15] is an extension of the well-known aeroelastic tool OpenFAST and considers the interaction of turbines in a park. $\mathrm{DWM_{NREL}}$

[1] $L = D/8$, where L is the length scale of the spectral velocity tensor and D is the turbine diameter, opposed to L =33.6 m which is recommended for atmospheric turbulence above 60 m [6].

is built on the same principles as the original DWM model, with a meandering axisymmetric wake deficit obtained from a modified eddy viscosity closure and a near-wake correction model. However, some of the simplifications in the $\mathrm{DWM}_{\mathrm{DTU,\ Mann}}$ model have been addressed. The quasi-steady wake deficit in $\mathrm{DWM}_{\mathrm{DTU,\ Mann}}$ is restricted to only meander in two dimensions (crosswise and vertical), and its streamwise position is only a function of its transport velocity, which equals the freestream velocity. In $\mathrm{DWM}_{\mathrm{NREL}}$, the wake can also meander in the streamwise direction, and the transport velocity of the wake deficits equals the local wake velocity and is therefore a function of time. In addition, tilt and yaw misalignment of the rotor are accounted for and affects wake deflection. For handling multiple upstream wakes, a root-sum-square wake deficit summation method is used in $\mathrm{DWM}_{\mathrm{NREL}}$ for all inflow conditions, where the wakes of each upstream turbine are calculated sequentially [16]. Wake-added turbulence and a curled wake model due to tilt and yaw misalignment are recent improvements in $\mathrm{DWM}_{\mathrm{NREL}}$ but are not used in this study.

The third wake model included for comparison in this study is WIFET Farm [10]. This model is newly developed in the NEXTFARM project and is an extension to the aeroelastic tool 3DFloat [17]. As for $\mathrm{DWM}_{\mathrm{NREL}}$, $\mathrm{DWM}_{\mathrm{IFE}}$ is highly inspired by the original DWM framework but also has some differences. Instead of obtaining the initial velocity profile behind the turbine from the BEM model, $\mathrm{DWM}_{\mathrm{IFE}}$ assumes a Gaussian wake deficit profile for all positions downstream of the turbine. However, the blade forces are obtained from BEM when coupled to 3DFloat. An initial center-line velocity deficit is applied $2D$ downstream of the turbine, while the magnitude of this deficit is a function of TI in the ambient flow and the rotor thrust coefficient, c_T, as suggested by [18]. $c_T(U)$ is obtained from look-up tables for the specific turbine. The transport velocity of the wake deficits is approximated to 80 % of the freestream velocity, which has been shown to be a good compromise for a range of inflow conditions [7]. For multiple wake situations, a momentum-conserving velocity deficit summation method is used [19]. Instead of accounting for wake meandering in a statistical sense [9] as first implemented in the WIFET Farm model [10], we present in this paper results where the meandering is treated similarly as in the original DWM model. Then $\mathrm{DWM}_{\mathrm{IFE}}$ is no longer restricted to only account for the effect of meandering on the time-averaged velocity field but obtain time-realizations of wake meandering necessary for load calculations. $\mathrm{DWM}_{\mathrm{IFE}}$ does not include a wake-added turbulence model for load calculations analogous to the one formulated in the original DWM model. However, the increased TI in the wake due to the turbulence-generating wake deficit shear is modeled based on the eddy viscosity formulation in the wake-deficit model, and the total contribution of increased TI from all upstream wakes is estimated by a root-sum-square summation. Thus, the increased effective TI felt by a turbine under waked conditions is taken into account and affects the development of its own wake downstream.

The main differences between the three DWM model implementations are summarized in table 1.

2.2. Large-eddy simulations

The LES reference case is (called $\mathrm{LES}_{\mathrm{UU}}$ in this study) computed with the numerical framework EllipSys3D [20, 21, 22]. The solver has been used in numerous wind-power-related studies including fundamental investigations of atmospheric boundary layer (ABL) flows and wind turbine wakes [23, 24, 25, 26]. LES in general is a popular choice as a reference dataset against which to validate and calibrate DWM models [5, 15, 27, 26].

The governing equations are formulated in a collocated finite-volume approach and solved with the SIMPLE algorithm. The diffusive terms are discretized by second-order central differences. A blend of third-order QUICK (10 %) and fourth-order central differences (90 %) is used for the advection terms. Pressure decoupling is avoided using the Rhie-Chow interpolation. The sub-grid scales are modeled with the formulation by Deardorff [28].

Table 1: Main DWM building blocks

	DTU (DWM + HAWC2)	NREL (FAST.Farm)	IFE (WIFET)
Initial wake	BEM	BEM	$c_T(U)$ tables/ Gaussian profile
Eddy viscosity closure	Ambient + wake deficit	Ambient + wake deficit	Ambient + wake deficit
Wake transport velocity	U_∞	Local velocity	$0.8U_\infty$
Meandering direction	y and z	All directions	y and z
Wake summation	Max deficit/linear (below/above rated)	Root-sum-squared locally and sequential globally	Momentum conserving
Correct for tilt and yaw misalignment	Only in load calculations	In load calculations and flow	Only in load calculations
Wake added turbulence	Yes	Forthcoming	No
Wake-turbulence build-up	No	No	Yes
Ground effects	Can be included	No	Yes

The inflow is generated in a bi-periodic precursor simulation of a pressure-driven isothermal boundary layer. The domain measures $L_z = 1280\,\mathrm{m}$ in the vertical, and $L_{x,y} = \{6, 4\}\, L_z$ in the streamwise and lateral directions. The grid is uniform with $\Delta x = 20\,\mathrm{m}$ and $\Delta y = \Delta z = 10\,\mathrm{m}$. A symmetry boundary condition is applied at the top. At the bottom, the surface shear stress is prescribed using the Monin-Obukhov similarity theory [29] and the local instantaneous velocity sampled at the first grid point above the boundary. The driving pressure gradient is set to $\partial p/\partial x = -\rho\, u_*^2/L_z$ with a friction velocity $u^* = 0.44\,\mathrm{m/s}$. The surface roughness is set to $z_0 = 0.000\,11\,\mathrm{m}$. Inflow data for the main wind farm simulation are sampled after an initial spin-up time of 30 000 s.

The domain of the main simulation (i.e., the simulation with the wind turbines) has the same dimensions $L_{x,y,z}$ as the precursor. The first turbine is located $6D$ downstream of the inlet. The grid in the turbine and wake region is uniform with a cell width $\Delta x = \Delta y = \Delta z = D/32 = 3.9375\,\mathrm{m}$ starting $3D$ upstream of the first turbine and extending $21D$ downstream. It comprises $4D$ in the lateral and vertical directions. Away from the inner region the grid is continuously stretched towards the boundaries. The turbine rotors in the main simulation are represented by actuator line models (ALMs) [23]. In the ALM the blades are discretized in terms of 32 blade elements. The body forces of the ALM are projected to the grid with a standard three-dimensional Gaussian smearing function with a smearing width of $\epsilon = 2\Delta x$. Spurious induction effects due to the finite core-size of the root and tip vortices are corrected with the smearing correction by Meyer-Forsting *et al.* [30]. After an initial spin-up of 30 min, the main simulation is run for 1h.

2.3. Test case

In this study we consider a row of four NREL 5MW reference turbines [31] spaced $7.5D$ apart in line with the incoming wind. The NREL 5MW turbine has a rotor diameter of $D = 126\,\mathrm{m}$,

hub height of 90 m, a rated speed of 11.4 m/s, and a rated aerodynamic power of 5.3 MW. As this study aims to investigate the differences in the wake models and their isolated impact on power and loads, we have attempted to exclude the effect from other parts of the park models. Therefore, it was decided to use the same incoming wind field for all models, the LES-generated precursor described in the previous section, with a time-averaged velocity $U = 14.12\,\mathrm{m/s}$, turbulence intensity $TI = 5.03\ \%$ and integral length scale $L \approx 255\,\mathrm{m} \approx 2D$ at hub height. The Mann box used with $\mathrm{DWM_{DTU,\ Mann}}$ is scaled to have the same TI as the LES precursor, while the integral length scale is estimated to be $L \approx 112\,\mathrm{m} \approx 0.9D$. The inflow case in this study represents above-rated wind speed conditions with rather low TI relevant for offshore sites. The inflow data provided to the DWM models were sampled in a separate run of the main LES without turbines in a plane $1D$ upstream of the position of the first turbine. This way, it is ensured that the inflows seen by the turbines were as similar as possible. For the DWM simulations, the LES-generated wind field was then imposed $1D$ in front of turbine 1, and the simulations were run for 52.5 min. To exclude any transient effects in the beginning of the simulations, the first 7.5 min of the simulations were excluded, resulting in an effective simulation length of $t_{\mathrm{sim}} = 45\,\mathrm{min} \approx 5L_x/U_\infty$.

In all simulations, the turbines were forced to operate at fixed rotor speed and blade pitch. The rotor speed was set to 12.1 RPM for all turbines, and the blade pitch were set to 8.92°, 6.71°, 4.95°, and 3.53°, respectively, for turbines 1 to 4. These predefined values were set by first running the $\mathrm{DWM_{IFE}}$ model with variable rotor speeds and blade pitch with the same inflow and using the time-averaged values from this run for the final simulations. However, the approach for $\mathrm{DWM_{DTU,\ Mann}}$ and $\mathrm{DWM_{DTU}}$ is to run all upstream wake-generating turbines at free inflow conditions, except the turbine where the loads are simulated. So when the loads of turbine 4 were simulated, turbines 1 to 3 were set to rotor speeds of 12.1 RPM and the blade pitch at 8.92°, while turbine 4 was set to 12.1 RPM and blade pitch at 3.53°.

To get results comparable to the $\mathrm{LES_{UU}}$, it was decided to run the aeroelastic solvers coupled to the DWM wake models with rigid rotors and exclude all the effects from the tower. Aerodynamic forces along the radial span of the blade were reported from all the simulations, and power and loads were calculated from these forces using the same algorithms.

3. Results

3.1. Mean velocity profiles

Figure 1 shows time-averaged velocity profiles at three axial positions, $-1D$, $2.5D$, and $5D$, relative to the four turbines. The DWM models show symmetric horizontal velocity profiles for all positions, whereas in the LES case, the maximum is slightly shifted to the right (looking from upstream). Since Coriolis forces were not considered in this study, this shift is likely to be related to the asymmetric entrainment of momentum due to the rotation of the wake [32]. The $\mathrm{LES_{UU}}$ wake behind turbine 1 clearly moves upwards (see vertical profile at $x_{t=2} = -D$), which can be the result of wake rotation, but also the tilt angle of the rotor deflects the wake upwards. For the downstream turbines this wake displacement is also present but not as pronounced. For $\mathrm{DWM_{NREL}}$, which is the only DWM model that includes the effect of wake deflection as a result of tilt and yaw misalignment, this wake displacement is less clear than in the $\mathrm{LES_{UU}}$. This can be due to the missing wake rotation model in this version of $\mathrm{DWM_{NREL}}$, or simply because the wake deficits of $\mathrm{DWM_{NREL}}$ are considerably weaker than $\mathrm{LES_{UU}}$.

While $\mathrm{DWM_{IFE}}$ assumes a Gaussian wake deficit profile for all x, the velocity deficit profiles for $\mathrm{LES_{UU}}$, $\mathrm{DWM_{DTU}}$ and $\mathrm{DWM_{NREL}}$ develop towards a Gaussian profile as the wake moves downstream. For turbine 1, $\mathrm{LES_{UU}}$ is the only model that shows two distinct peaks in the velocity deficit at $x_{t=1}/D = 2.5$, with the right peak stronger than the left. While this shape is not visible in the wake of any of the other turbines for the $\mathrm{LES_{UU}}$, likely due to a faster wake recovery caused by the higher TI in the wake, the wake shape with two peaks is more

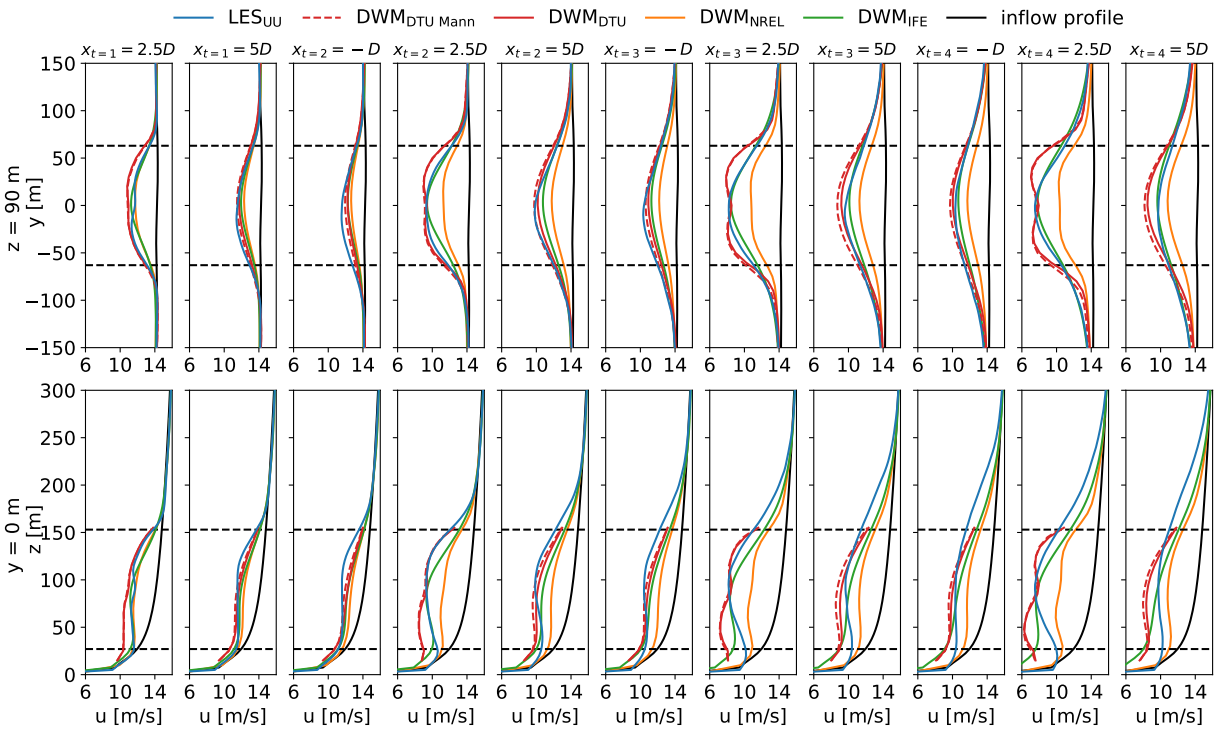

Figure 1: Time-averaged velocity profiles, at axial positions $-D$, $2.5D$, and $5D$, relative to the four turbines. The subscript in x_t denotes the turbine number. Dashed horizontal lines indicate the range of the turbine rotor's swept area.

pronounced for DWM$_{\mathrm{NREL}}$ and especially the two DTU DWM models. In general, DWM$_{\mathrm{NREL}}$ tends to underpredict the wake deficit, especially in the near-wake ($x/D = 2.5$) of turbines 2–4. DWM$_{\mathrm{IFE}}$ and DWM$_{\mathrm{DTU}}$ match well with LES$_{\mathrm{UU}}$ but show a faster attenuation of the wake. For DWM$_{\mathrm{DTU}}$ the wake builds up more than for the other models, which results in an overprediction of the deficit for turbine 4 compared to LES$_{\mathrm{UU}}$.

Some of the model differences we see in the wake deficits are likely due to the turbines running at constant rotor speeds and blade pitch angles set by the DWM$_{\mathrm{IFE}}$ model that are not the ideal speeds and angles that the other models would have naturally predicted under these waked conditions. That is, differences in the rotor aerodynamic modeling between the software may be playing a sizeable role, in addition to differences in wake modeling.

The vertical profile of DWM$_{\mathrm{IFE}}$ differs in shape with higher deficit in the lower part of the wake and lower deficit in the higher part of the wake including above the rotor span. This can also partly be seen for DWM$_{\mathrm{DTU}}$. For the case of DWM$_{\mathrm{IFE}}$, the ground effect causes the velocity near the ground in the waked flow to decrease.

Finally, it should be noted that the mean velocity profiles from the two DTU DWM simulations are close, with DWM$_{\mathrm{DTU,\ Mann}}$ showing slightly stronger deficits than DWM$_{\mathrm{DTU}}$. However, the turbulence (not shown here) and load generation as will be seen later are quite different.

3.2. Power and thrust

Figure 2 shows time-averaged aerodynamic thrust force and power for the four turbines investigated. While all models show excellent agreement for turbine 1 (except DWM$_{\mathrm{NREL}}$ that

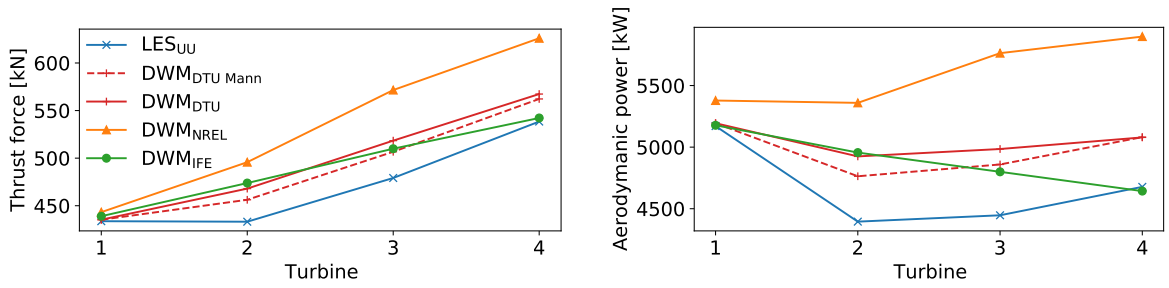

(a) (b)

Figure 2: (a) Aerodynamic thrust force and (b) aerodynamic power, averaged over 45 min. Note that the y axes have different scales and do not start from zero.

predicts about 4 % higher power than the other models), the DWM models generally predict higher power and thrust than LES$_{UU}$ for the rest of the turbines. DWM$_{DTU}$, DWM$_{DTU,\ Mann}$, and especially DWM$_{NREL}$ show higher values for all waked turbines. DWM$_{IFE}$ shows higher values for turbines 2 and 3 compared to LES$_{UU}$.

What is maybe a more interesting aspect than how the absolute values of thrust and power compare between the models is the development along the row of turbines. LES$_{UU}$ shows a different development than especially DWM$_{IFE}$ that has a linear development of thrust and power for the whole row. DWM$_{NREL}$ and the two DTU DWM simulations seem to partly capture the breaking point seen for LES$_{UU}$ at turbine 2, and have similar rates of change downstream of this point.

In general, there is a good correlation between the estimation of wake deficits for the different models and their prediction of thrust and power. It is also worth pointing out that DWM$_{NREL}$ predicts higher power than rated for some of the turbines. This is again probably a result of the predefined constant rotor speeds and blade pitch angles different from what DWM$_{NREL}$ would have naturally predicted under these waked conditions.

3.3. Blade forces

All the DWM models capture shapes of the time-averaged tangential and normal force distributions along the blade span (not shown) in very good agreement with LES$_{UU}$. The magnitudes, however, change proportionally to the integrated values in figure 2 from turbine 1 to 4. Also, the deviations between the models increase along the turbine row.

Figure 3 shows the time-averaged azimuthal variation of the normal component of the blade force at four radial positions along the blade for the turbines in the row. The time-averaged normal force at each radial position, $\bar{F}_n$, is subtracted from the blade forces, $\bar{F}_n^\phi$, which are azimuthally binned with $\Delta\phi = 12°$ over all blade rotations of the 45 min simulations, and as a result only the force variation the blade experiences over the rotation is shown. Finally, $\bar{F}_n^\phi - \bar{F}_n$ is normalized by $\bar{F}_n$. With minor differences between the models, the maximum blade force for turbine 1 occurs around $\phi = 0°$. This is when the blade points upwards, which, due to the incoming shear flow, corresponds to when the blade experiences the highest wind. Equivalently, the minimum blade force occurs around $\phi = 180°$. All models show increasing amplitudes in force variation towards the blade tip for all turbines, which is consistent with the velocity difference felt by the blade sections over a rotation for a blade operating in sheared flow.

The shape of the force variations shows good agreement between the DWM models for all turbines, even though DWM$_{NREL}$ and the two DTU DWM simulations seem to be slightly shifted towards higher ϕ. LES$_{UU}$, however, shows a clear phase shift towards lower ϕ for the

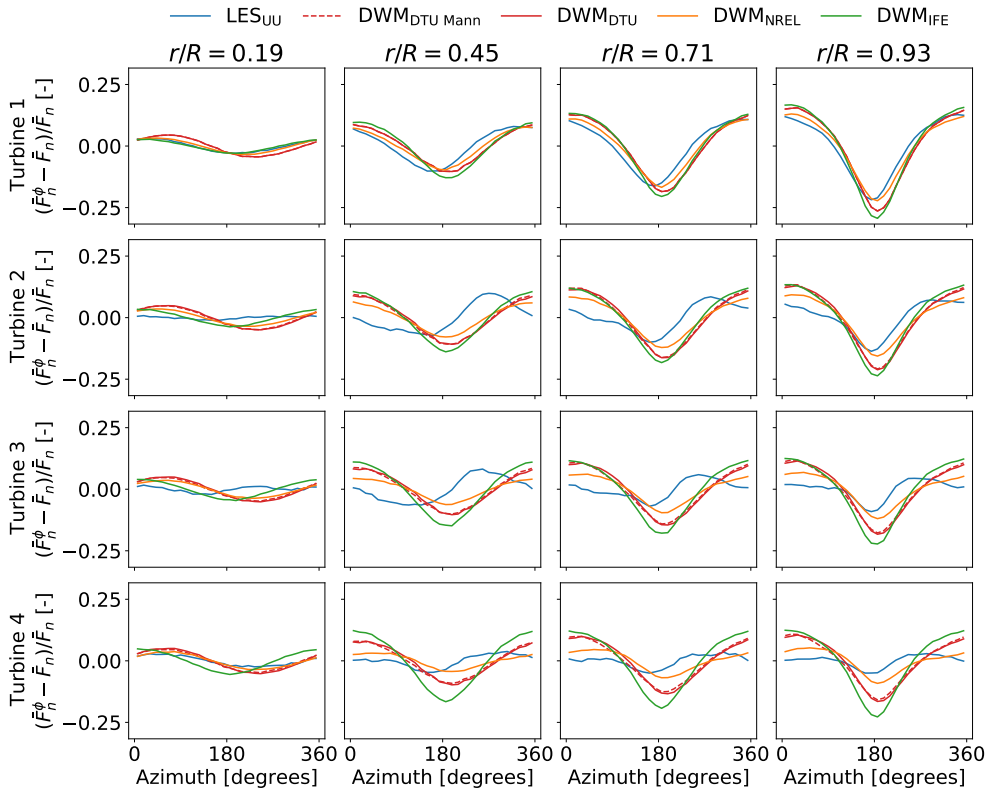

Figure 3: Difference between mean normal blade force per azimuthal bin $\bar{F}_n^\phi$ ($\Delta\phi = 12°$) and total normal force $\bar{F}_n$.

waked turbines. This shift seems to increase further into the turbine row, and the force variation also changes shape. For turbine 4 the maxima occur at $\sim 270°$ and the minima at $\sim 175°$, and are results of the wakes moving slightly to the right (looking from upstream) and away from the ground, as was seen in figure 1. This shifts the area of highest wind felt by the blade to the left.

The amplitudes of the force variations deviate significantly between the models. LES$_{\mathrm{UU}}$ shows the lowest amplitudes for all turbines, while DWM$_{\mathrm{IFE}}$ shows the largest. It is also interesting to note that while the amplitude of the force variation stays approximately constant for all turbines for DWM$_{\mathrm{DTU}}$ it increases slightly for DWM$_{\mathrm{IFE}}$ and decreases deeper into the turbine row for LES$_{\mathrm{UU}}$ and DWM$_{\mathrm{NREL}}$. To understand the deviations between the models, we go back to the time-averaged velocity profiles given in figure 1. For all models, turbine 1 experiences the same incoming wind shear profile, so here the deviations are only due to the differences in the turbine model. For this turbine there is a good agreement between the models for the three radial positions closest to the blade root, while the differences at $r/R = 0.93$ can be due to differences in the blade tip correction method. For the other turbines, the blade forces are affected by varying incoming wind, which originates from deviations in wake simulations. As an example, we can look at the vertical profile at $x_{t=4} = -D$ in figure 1, where the velocity difference between the lower and upper part of the blade span is larger for DWM$_{\mathrm{IFE}}$ than LES$_{\mathrm{UU}}$, with DWM$_{\mathrm{DTU}}$ and DWM$_{\mathrm{NREL}}$ being somewhere in between. This coincides with the force variation for turbine 4, where DWM$_{\mathrm{IFE}}$ has the highest and LES$_{\mathrm{UU}}$ the lowest amplitudes. For the case of DWM$_{\mathrm{IFE}}$, the ground effect amplifies the velocity difference felt by the rotating blade. For LES$_{\mathrm{UU}}$, on the

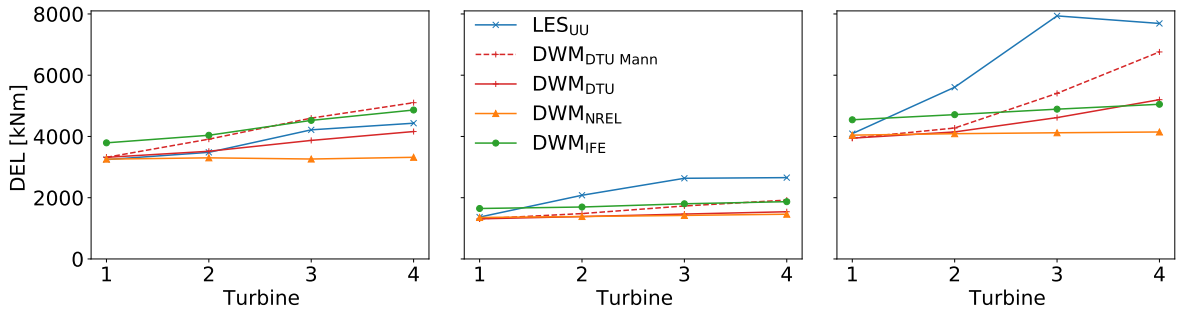

(a) (b) (c)

Figure 4: DELs of (a) blade root flapwise bending moment, (b) tower top yaw bending moment and (c) tower base fore-aft bending moment.

other hand, the time-averaged wake moves slightly upwards, causing the incoming velocity for the waked turbines to have a flatter profile compared to the undisturbed flow.

3.4. Fatigue

Figure 4 shows 45 min damage equivalent loads (DELs) of (a) blade root flapwise bending moment, (b) tower top yaw bending moment, and (c) tower base fore-aft bending moment. Wöhler coefficients of 10 and 3 are used for the blades and tower, respectively. Further details on the DEL calculations can be found in [33]. For the DELs investigated, there is an excellent match between the models for turbine 1, except for $\mathrm{DWM_{IFE}}$ estimating 14–24 % higher DELs than the rest. With some variation, $\mathrm{LES_{UU}}$ shows a considerable increase in DELs from turbines 1 to 3, and then only small changes from turbines 3 to 4. For the blade root flapwise bending moments, the two DTU DWM simulations and $\mathrm{DWM_{IFE}}$ are closest to $\mathrm{LES_{UU}}$ in the development along the turbine row, whereas $\mathrm{DWM_{NREL}}$ shows only minor changes from turbines 1 to 4. For the tower moments, $\mathrm{DWM_{NREL}}$ and $\mathrm{DWM_{IFE}}$ estimate almost no change in DELs along the turbine row, likely due to the lack of wake-added turbulence in these models. For $\mathrm{DWM_{DTU}}$ and even more for $\mathrm{DWM_{DTU,\ Mann}}$, there is an increase in tower DELs from turbines 1 to 4.

For a deeper investigation of the differences in DELs, we can investigate the power spectral density (PSD) of the loads. In figure 5 this is presented as cumulative integrals for blade root flapwise bending moments and tower base fore-aft bending moments. For both blade and tower loads, all models except $\mathrm{DWM_{NREL}}$ show increasing levels of energy below f_c along the turbine row, where f_c is the cut-off frequency of the large-scale turbulence responsible for wake meandering[2]. It is in this frequency range the load variations associated with wake meandering are expected to appear. $\mathrm{DWM_{DTU,\ Mann}}$, which opposed to the other simulations uses Mann turbulence for wake meandering, shows a significantly larger increase in energy below f_c along the turbine row compared to $\mathrm{DWM_{DTU}}$. This suggests that the increased load generation of the $\mathrm{DWM_{DTU,\ Mann}}$ model is due to an increased meandering deriving it from the Mann box with a $1D$ grid size, and the deeper deficit using the original parameter settings in the model for computing the eddy viscosity. This low-frequency part of the spectra is dominating the tower load spectra, in particular for $\mathrm{DWM_{DTU,\ Mann}}$. For the simulations where the LES precursor turbulence drives the meandering (all except $\mathrm{DWM_{DTU,\ Mann}}$), the differences in energy below f_c can be explained by variations in wake model implementation. $\mathrm{DWM_{DTU}}$ uses a wake transport

[2] f_c was originally specified as $\frac{U_\infty}{2D_w}$ [4], where D_w is the instantaneous wake deficit diameter. Since D_w varies with downstream position, we have here approximated the cut-off frequency to be $f_c = \frac{U_\infty}{2D} > \frac{U_\infty}{2D_w}$, which is a upper limit for the frequencies associated with wake meandering valid for all downstream positions.

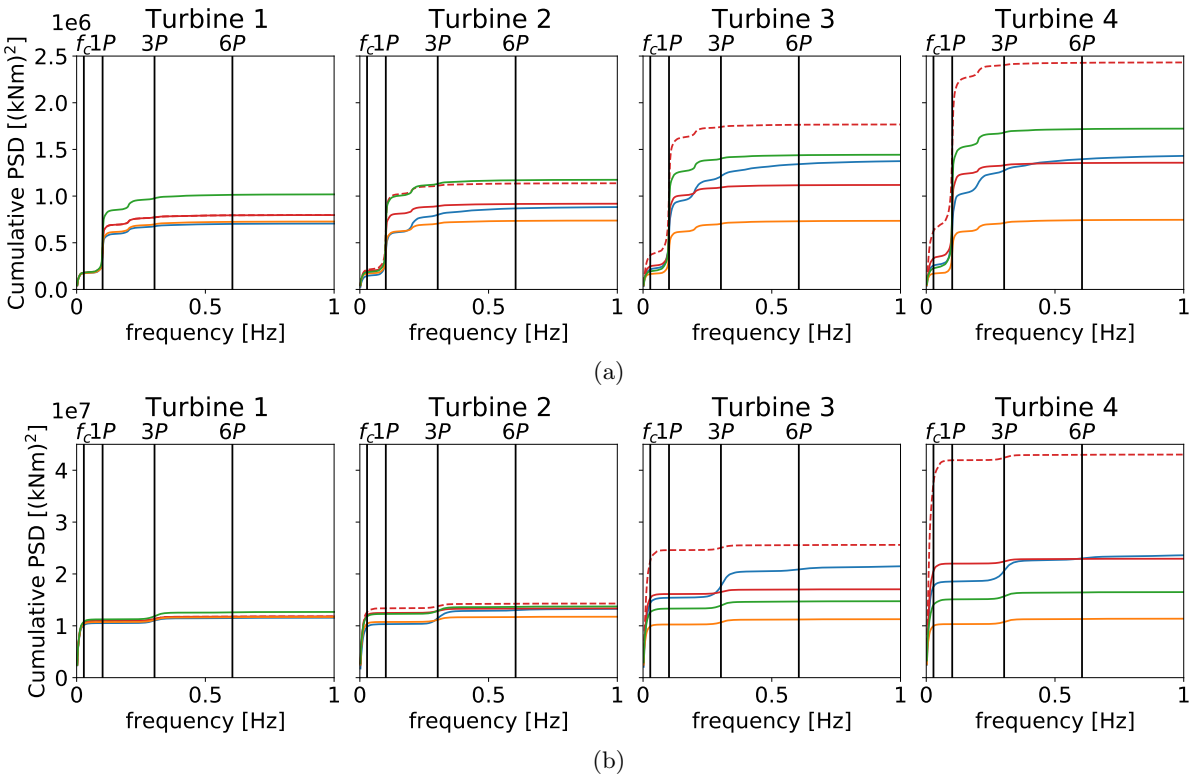

Figure 5: Cumulative integrals of PSD of (a) blade root flapwise bending moment and (b) tower base fore-aft bending moment. For legends, see figure 3.

velocity of U_∞, which has shown to result in more meandering movement in the far wake compared to a lower wake transport velocity used by the other models [7]. This coincides with $\mathrm{DWM_{DTU}}$ showing more energy below f_c compared to the other models for turbines 3 and 4, where the wakes of their upstream turbines have moved far in the downstream direction. $\mathrm{LES_{UU}}$, on the other hand, is the only simulation where the increased turbulence levels in the wake flow contribute to meandering of the downstream wakes, and explains the increased energy below f_c for turbines 3 and 4.

The cumulative integrals of blade root moment PSD in figure 5a show jumps at $1P$ and higher harmonics for all models. These jumps are equivalent to the peaks in a non-integrated PSD plot. The $1P$ frequency corresponds to the rotational speed of the turbines, and the peak at this frequency comes from the blade force variation over a rotation shown in figure 3. As this variation is not completely sinusoidal, energy at higher harmonics ($2P$, $3P$) are also seen. However, the energy content at these harmonics quickly drops as the frequency increases.

For turbine 1, $\mathrm{DWM_{IFE}}$ shows the largest energy jumps at $1P$, while all models show similar jumps at $2P$ and $3P$, and negligible energy above this frequency. For the DWM simulations using the LES precursor turbulence, the jumps at $1P$ scales well with the force variation the blades experience over a rotation. $\mathrm{DWM_{IFE}}$ shows largest energy content at $1P$, while $\mathrm{DWM_{DTU}}$ shows second largest energy content around this frequency. For both of these DWM models, the jumps at $1P$ grow further into the turbine row. $\mathrm{DWM_{NREL}}$, however, shows only minor changes for the $1P$ frequency from turbines 1 to 4. For $\mathrm{DWM_{DTU,\ Mann}}$ and $\mathrm{LES_{UU}}$, the jumps at $1P$ do not scale with the force variation seen in figure 3. $\mathrm{DWM_{DTU,\ Mann}}$ shows a significantly larger increase in $1P$ energy along the turbine row compared to $\mathrm{DWM_{DTU}}$, even though the blade force variation is close to identical for the two simulations. For $\mathrm{LES_{UU}}$, figure 3 shows

decreasing force variation along the turbine row, while the blade load spectra show larger jumps at $1P$ for turbines 3 and 4 compared to turbines 1 and 2. The mismatch between the blade force variation seen in figure 3 and the $1P$ energy is likely due to wake meandering, which is significantly stronger for $\mathrm{DWM_{DTU,\ Mann}}$ and $\mathrm{LES_{UU}}$. This slow motion of the upstream wakes normal to the wind causes additional velocity gradients to appear when a wake hits parts of the downstream turbines' swept rotor area. Since $f_c < 1P$, these gradients normally last for several blade rotations, but the effect will be averaged out in figure 3.

The DWM models show negligible energy above $3P$ for the waked turbines, which was also seen for turbine 1. $\mathrm{LES_{UU}}$, however, shows increased energy content above $1P$ along the turbine row. This is likely due to higher increase in TI in the $\mathrm{LES_{UU}}$ wakes compared to the DWM models. This development along the turbine row agrees with the trend in DELs for $\mathrm{LES_{UU}}$ that was seen in figure 4.

The tower loads, represented by the tower base fore-aft moments in figure 5b, show jumps at the $3P$ frequency for all models, and for the harmonic $6P$ for $\mathrm{LES_{UU}}$. $3P$ is the period of the load variation felt by the tower due to the rotation of the three-bladed rotor, and the energy at the harmonics come from the non-sinusoidal behavior of this variation. $\mathrm{DWM_{IFE}}$ shows slightly higher jumps at the $3P$ frequency compared to the other DWM models for all turbines, and also compared to $\mathrm{LES_{UU}}$ for turbine 1. This originates from the higher $1P$ force variation felt by each blade $\mathrm{DWM_{IFE}}$ showed in figure 3 and explains why this model estimates larger DELs for turbine 1. For the waked turbines, $\mathrm{LES_{UU}}$ shows more energy at $3P$ and higher frequencies compared to the DWM models, and the energy in this region increases along the turbine row.

4. Conclusions

In this study, we have compared the performance of three models based on the DWM approach with LES ALM simulations, when predicting wake flow, power and loads on a row of four turbines. $\mathrm{DWM_{IFE}}$ has shown good agreement to $\mathrm{LES_{UU}}$ comparing the time-averaged results, especially for turbine 1. For turbines 2 and 3, too-low wake deficits were estimated compared to $\mathrm{LES_{UU}}$, resulting in higher power and thrust for these turbines. For turbine 4 the agreement between $\mathrm{DWM_{IFE}}$ and $\mathrm{LES_{UU}}$ is again good, but the models are predicting different trends along the turbine row, especially for aerodynamic power. $\mathrm{DWM_{NREL}}$ estimates in general too-low wake deficits, causing power and thrust to be overestimated for the waked turbines. $\mathrm{DWM_{DTU}}$, on the other hand, estimates high deficits in the near-wake of the turbines, but also faster recovery of the wakes, causing both power and thrust to be overestimated for the waked turbines compared to $\mathrm{LES_{UU}}$.

All the models showed fairly good agreement when comparing fatigue loads of blade root moments, with deviations within 25 % of the estimations by the $\mathrm{LES_{UU}}$ reference case. All models except $\mathrm{DWM_{NREL}}$ showed an increase in DELs along the turbine row. However, for the DWM models it seems like the development in blade root moment DELs is predominantly driven by the energy content at the $1P$ frequency, which again scales well with the force variation the blades experience over a rotation when the effect of meandering is small. For $\mathrm{LES_{UU}}$ the increase in $1P$ energy due to meandering, and in energy at higher frequencies ($>1P$) is the key driver for the blade root loads and also the tower loads, causing the DELs to increase even though the average blade force variation decreases. For the tower loads, and especially the tower base fore-aft moments, all the DWM models highly underestimate the DELs deeper into the turbine row, except for $\mathrm{DWM_{DTU,\ Mann}}$ that shows some increase along the row. This aspect should, however, be investigated further by for example comparing the DWM models against full-scale data, as there is an uncertainty in the use of the rigid rotor models for load calculations.

One key finding in this study is the importance of accurate modeling of the shape of the vertical velocity profile and the meandering level, which highly influence the $1P$ variation in the blade loads. For $\mathrm{DWM_{IFE}}$ this certainly can be improved, and several parts of the wake model,

including ground effects, the assumption of axisymmetric and Gaussian-shaped wake deficit and lack of wake deflection, should be revised. Another key finding is that the DWM models do not capture the increased meandering and the increased energy at frequencies above $1P$ seen in the load spectra for the waked turbines for $\mathrm{LES_{UU}}$, which seems to be the main driver for increased fatigue on the turbines deeper into the row. This effect might be captured by a wake-added turbulence model. In that case a modification to the original wake-added turbulence model should be considered, as $\mathrm{DWM_{DTU}}$ did not capture the same wake effects on the fatigue loads, as was seen in the $\mathrm{LES_{UU}}$.

Acknowledgments

This work has been funded by the Norwegian Research Council, through the project NEXTFARM - Engineering speed modeling of realistic fatigue for all the individual turbines in wind parks by representative pre-calculations, Grant No. 281020. The LES computation was enabled by resources provided by the Swedish National Infrastructure for Computing (SNIC), partially funded by the Swedish Research Council through grant agreement no. 2018-05973. This work was authored in part by the National Renewable Energy Laboratory, operated by Alliance for Sustainable Energy, LLC, for the U.S. Department of Energy (DOE) under Contract No. DE-AC36-08GO28308. Support for the work was also provided by the Institute for Energy Technology under Agreement TSA-22-23308. The views expressed in the article do not necessarily represent the views of the DOE or the U.S. Government. The U.S. Government retains and the publisher, by accepting the article for publication, acknowledges that the U.S. Government retains a nonexclusive, paid-up, irrevocable, worldwide license to publish or reproduce the published form of this work, or allow others to do so, for U.S. Government purposes.

References

[1] Jensen N O 1983 *A note on wind generator interaction* (Roskilde)
[2] Frandsen S 1992 *J. Wind Eng. and Industrial Aerodynamics* **39** 251–265
[3] Larsen T J, Larsen G C, Madsen H A and Petersen S M 2015 *EWEA Annual Conf. and Exh. 2015* 95–99
[4] Larsen G C, Madsen H A, Thomsen K and Larsen T J 2008 *Wind Energy* **11** 377–395
[5] Madsen H A, Larsen G C, Larsen T J, Troldborg N and Mikkelsen R 2010 *J. Solar Energy Eng.* **132** 041014
[6] IEC 2019 *IEC 61400-1 Ed 4: Wind energy generation systems - Part 1: Design requirements* (Geneva)
[7] Keck R E, Madsen H A, Larsen G C, Veldkamp D, Wedel-Heinen J J and Forsberg J 2013
[8] Jonkman J M, Annoni J, Hayman G, Jonkman B and Purkayastha A 2017 *35th Wind Energy Symp.* 0454
[9] Braunbehrens R and Segalini A 2019 *J. Wind Eng. and Industrial Aerodynamics* **193** 103954
[10] de Vaal J B and Muskulus M 2021 *J. Phys.: Conf. Series* **2018** 012012
[11] Mann J 1994 *J. fluid mechanics* **273** 141–168
[12] Mann J 1998 *Probabilistic engineering mechanics* **13** 269–282
[13] Larsen T J, Madsen H A, Larsen G C and Hansen K S 2013 *Wind Energy* **16** 605–624
[14] S Lissaman P B 1979 *J. Energy* **3** 323–328
[15] Jonkman J, Doubrawa P, Hamilton N, Annoni J and Fleming P 2018 *J. Phys.: Conf. Series* **1037** 062005
[16] Voutsinas S G, Rados K G and Zervos A 1990 *Proc. 1990 European Comm. Wind Energy Conf.* 181–5
[17] Nygaard T A, De Vaal J, Pierella F, Oggiano L and Stenbro R 2016 *Energy Procedia* **94** 425–433
[18] Ainslie J F 1988 *J. Wind Eng. and Industrial Aerodynamics* **27** 213–224
[19] Zong H and Porté-Agel F 2020 *J. Fluid Mechanics* **889**
[20] Michelsen J A 1992 *Basis3D - a platform for development of multiblock PDE solvers* (Lyngby)
[21] Michelsen J A 1994 *Block structured multigrid solution of 2D and 3D elliptic PDE's* (Lyngby)
[22] Sørensen N N 1995 *General purpose flow solver applied to flow over hills* (Roskilde)
[23] Sørensen J N and Shen W Z 2002 *J. Fluids Eng.* **124** 393–399
[24] Troldborg N, Sorensen J N and Mikkelsen R 2010 *Wind Energy* **13** 86–99
[25] Asmuth H, Olivares-Espinosa H, Nilsson K and Ivanell S 2019 *J. Phys.: Conf. Series* **1256** 012022
[26] Asmuth H, Diaz G P N, Madsen H A, Branlard E, Forsting A R M, Nilsson K, Jonkman J and Ivanell S 2022 *Renewable Energy* **191** 868–887
[27] Doubrawa P, Annoni J R and Jonkman J M 2018 *2018 Wind Energy Symp.*

[28] Deardorff J W 1980 *Boundary-Layer Meteorology* **18** 495–527
[29] Monin A S A M O 1954 *Nauk SSSR Geophiz. Inst* **24** 163–187
[30] Meyer Forsting A R, Pirrung G R and Ramos-García N 2019 *Wind Energy Science* **4** 369–383
[31] Jonkman J, Butterfield S, Musial W and Scott G 2009 *Definition of a 5-MW reference wind turbine for offshore system development* (Golden)
[32] Churchfield M J, Lee S, Michalakes J and Moriarty P J 2012 *J. turbulence* N14
[33] de Vaal J B, Nygaard T A and Stenbro R 2016 *J. Phys.: Conf. Series* **753** 042004